Supporting Information

Photochemical CO_2-reduction catalyzed by mono- and dinuclear phenanthroline-extended tetramesityl porphyrin complexes

Corinna Matlachowski[1] *and Matthias Schwalbe**[1]

[1] Institute of Chemistry, Humboldt-Universität zu Berlin, Brook-Taylor-St. 2, 12489 Berlin, Germany. Fax: +49-30-2093-6966; Tel: +49-30-2093-7571; *E-mail: matthias.schwalbe@hu-berlin.de

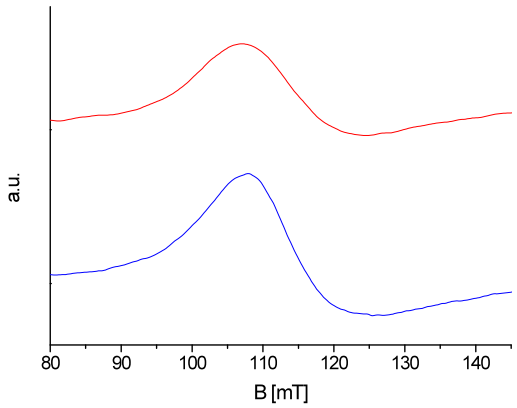

Figure S1. EPR-spectra of **Fe-1** (blue) and **Fe-1-Ru** (red) in DCM at 77 K, g = 6.0 for both.

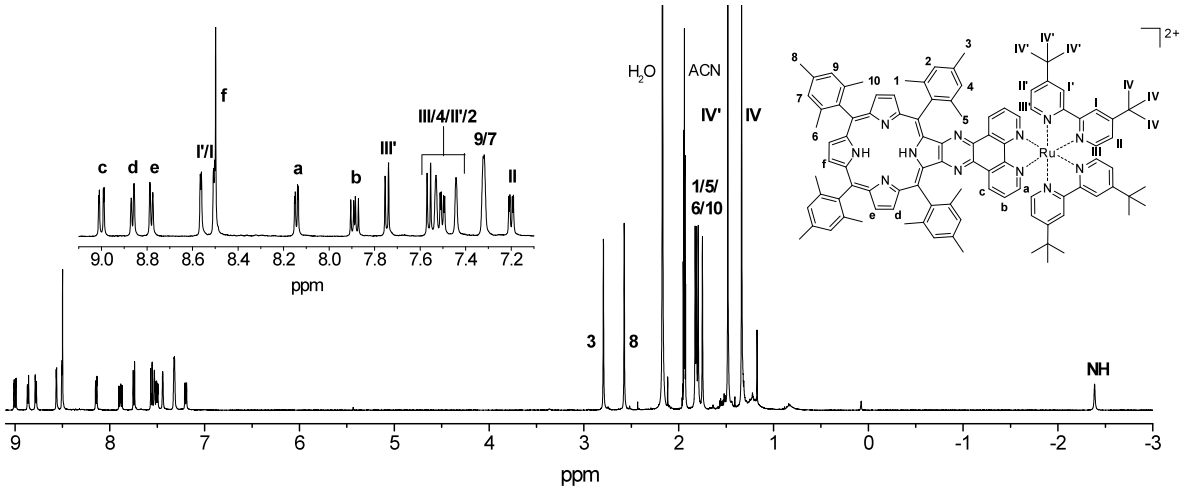

Figure S2. ^{1}H-NMR spectrum of **H_2-1-Ru** in CD_3CN (ACN = acetonitrile)

^{1}H NMR (400 MHz, CD_3CN, δ): -2.39 (s, 2H, NH), 1.34 (s, 18H, **IV**), 1.48 (s, 18H, **IV'**), 1.75-1.83 (m, 24H, **1,5,6,10**), 2.58 (s, 6H, **8**), 2.79 (s, 6H, **3**), 7.20 (dd, *J* = 1.5 and 4.8 Hz, 2H, **II**), 7.32 (s, 4H, **9/7**), 7.44 (s, 2H, **2**), 7.49-7.57 (m, 6H, **4,III,II'**), 7.75 (d, *J* = 5.0 Hz, 2H, **III'**), 7.89 (dd, *J* = 3.9 and 6.3 Hz, 2H, **b**), 8.14 (dd, *J* = 0.9 and 4.2 Hz, 2H, **a**), 8.50 (s, 2H, **f**), 8.51 (d, *J* = 1.5 Hz, 2H, **I** or **I'**), 8.57 (d, *J* = 1.5 Hz, 2H, **I** or **I'**), 8.78 (d, *J* = 3.6 Hz, 2H, **e**) 8.87 (d, *J* = 3.6 Hz, 2H, **d**), 9.00 (dd, *J* = 1.1 and 6.2 Hz, 2H, **c**)

Table S1. UV-Vis absorption maxima and emission maxima of **M-1** and **M-1-Ru** (**M** = H_2, Pd, Cu, Zn, Co, FeCl) in DCM

	Absorption maxima [nm] (ε/1000 [L/(mol*cm)])						**Emission maxima [nm]**
		Soret-band(s)		**Q-bands**			
H_2-1*		436(264.7)		527(25.0)	600(12.9)		655, 726
H_2-1-Ru	287(95.4)	428(140.1)		538(19.7)	608(12.7)	658(1.5)	665, 734
Cu-1*		408(108.8)	444(93.6)	525(6.5)	563(18.4)	601(8.2)	—
Cu-1-Ru*	286(78.1)	424(116.5)	472(67.5)	583(17.7)	633(sh, 4.1)		—
Pd-1*		403(89.8)	438(109.9)	507(4.9)	545(23.8)	579(11.7)	—
Pd-1-Ru*	287(71.5)	416(102.0)	460(69.3)	562(21.9)			—
Zn-1*		412(81.3)	446(89.8)	533(2.0)	570(14.2)	608(3.3)	615, 673
Co-1		411(99.3)		557(20.4)	587(17.4)		—
Co-1-Ru	287(92.4)	423(86.7)	470(76.4)	574(18.8)			—
FeCl-1		380(75.0)	438(100.4)	524(19.0)	734(sh, 3.2)		—
FeCl-1-Ru	287(83.6)	423(83.3)		530(sh, 22.3)	622(sh, 7.0)	690(sh, 4.0)	—

(*Matlachowski, C.; Schwalbe, M. *Dalton Trans*. **2013**, *42*, 3490-3503. Note that in this earlier article a wrong extinction coefficient for **H_2-1** had been published.)

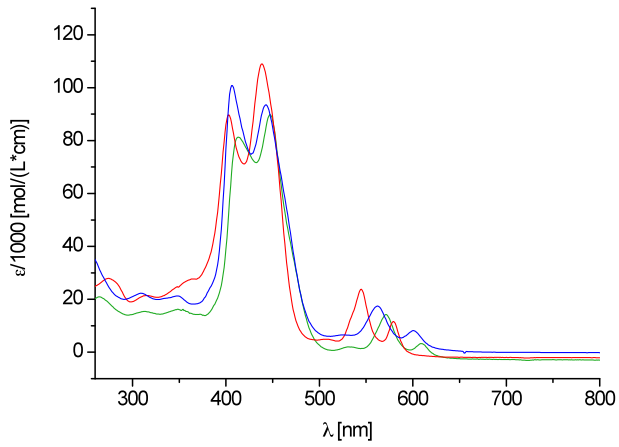

Figure S3. UV-Vis spectra of **Cu-1** (blue), **Pd-1** (red) and **Zn-1** (green) in DCM

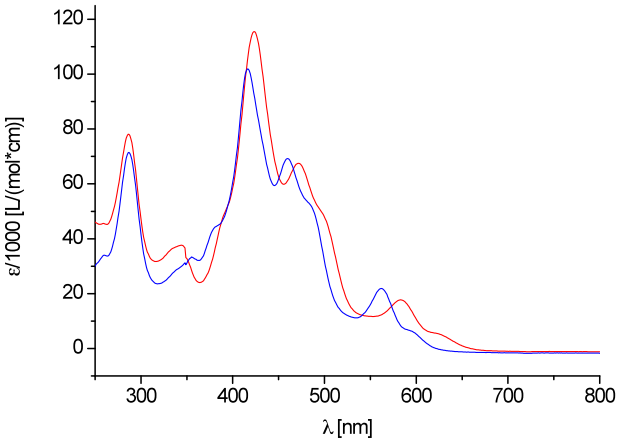

Figure S4. UV-Vis spectra of **Cu-1-Ru** (red) and **Pd-1-Ru** (red) in DCM

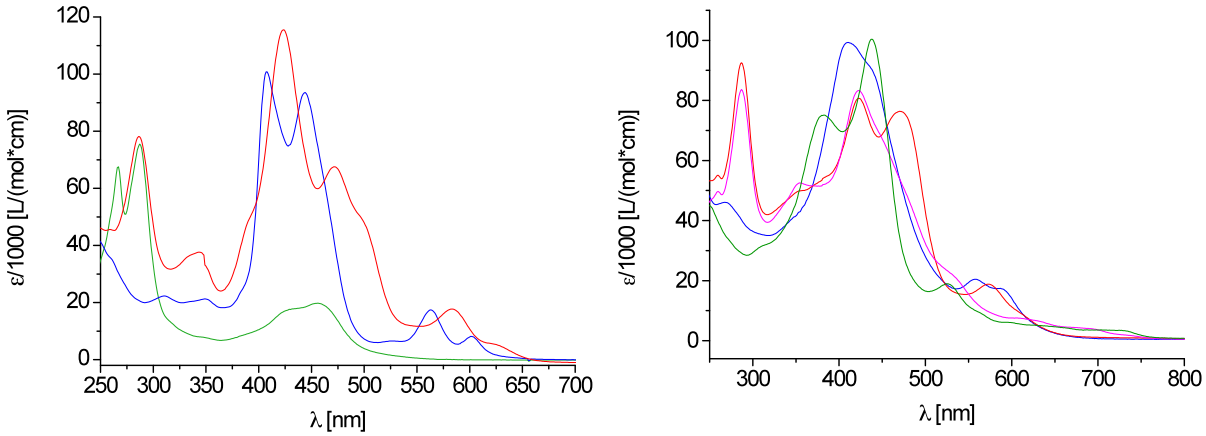

Figure S5: left: UV-Vis spectra of **Cu-1** (blue), **Cu-1-Ru** (red) and $[Ru(tbbpy)_2(phen)](PF_6)_2$ (green) and right: UV-Vis spectra of **Co-1** (blue), **Co-1-Ru** (red), **FeCl-1** (green) and **FeCl-1-Ru** (magenta) in DCM

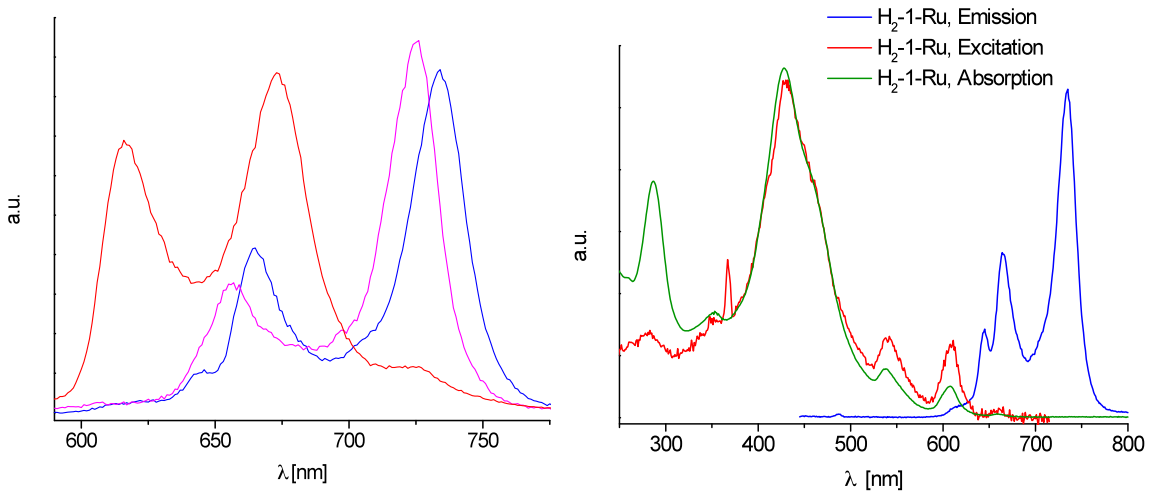

Figure S6. left: Emission profile of **Zn-1** (red), **H_2-**1 (magenta) and **H_2-1-Ru** (blue) (excitation wavelength in every case: 550 nm); right: absorption, emission (excitation wavelength: 435 nm) and excitation (measured at 735 nm) spectra of **H_2-1-Ru** in DCM

The excitation spectrum taken at the emission maximum at 735 nm matches very well with the absorption spectrum demonstrating that there are no individual complex moieties but rather a fully conjugated and interacting system that needs to be seen as its own entity.

Table S2. Redox potentials of **M-1** with **M** = Zn, Cu, Pd, H_2, Co und FeCl and **M-1-Ru** with **M** = Cu, Pd, H_2 in DCM containing 0.1M NBu_4PF_6 (TBAP)

	Potential vs Fc/Fc^+ in DCM						
Zn-1*	-2.25	-1.80			0.44	0.70	
Cu-1*	-2.21	-1.78			0.62	0.89	
Pd-1*	-2.25	-1.80			0.67	1.13	
H_2-1*	-2.01	-1.74			0.59		
Cu-1-Ru*	-2.16	-1.93	-1.57		0.60	0.88#	
Pd-1-Ru*	-2.09	-1.85	-1.50		0.76	0.91	
H_2-1-Ru	-1.95	-1.82	-1.54		0.66	0.85	1.03
$[Ru(tbbpy)_2(phen)](PF_6)_2$*	-2.08	-1.80				0.84	
Co-1	-2.25 $E_{p,c}$	-1.78	-1.25 $E_{p,c}$		0.51	0.79	
FeCl-1	-2.18 $E_{p,c}$	-1.47	-1.23	-0.84 $E_{p,c}$	0.72#	1.15	

*Matlachowski, C.; Schwalbe, M. *Dalton Trans*. **2013**, *42*, 3490-3503.

$E_{p,c}$ stands for cathodic peak potentials in case of irreversible reduction events. Note that almost all redox events of Fe-1-Ru und Co-1-Ru are irreversible and broad. Thus, determination and assignment of the events is very difficult and we do not denote the potentials here.

#2-electron processes because of overlapping events.

All cyclic voltammograms (CV) were performed on DCM solutions containing 0.1 M tetrabutylammonium hexafluorophosphate (TBAP) under argon atmosphere at ambient temperature. A potentiostat/galvanostat PGSTAT 101 from Metrohm was used to record CVs and square wave voltammograms (SQV). A three compartment cell was outfitted with a glassy carbon button electrode as the working electrode, a platinum wire as the auxiliary electrode, and a silver wire as a pseudo reference electrode. All data were referenced versus the ferrocene/ferrocenium couple at the end of each measurement. CVs were collected at scan rates of 20 - 800 mV/s. Square-wave voltammograms were collected at amplitude of 20 mV, step potential of 5 mV and a frequency of 25 Hz.

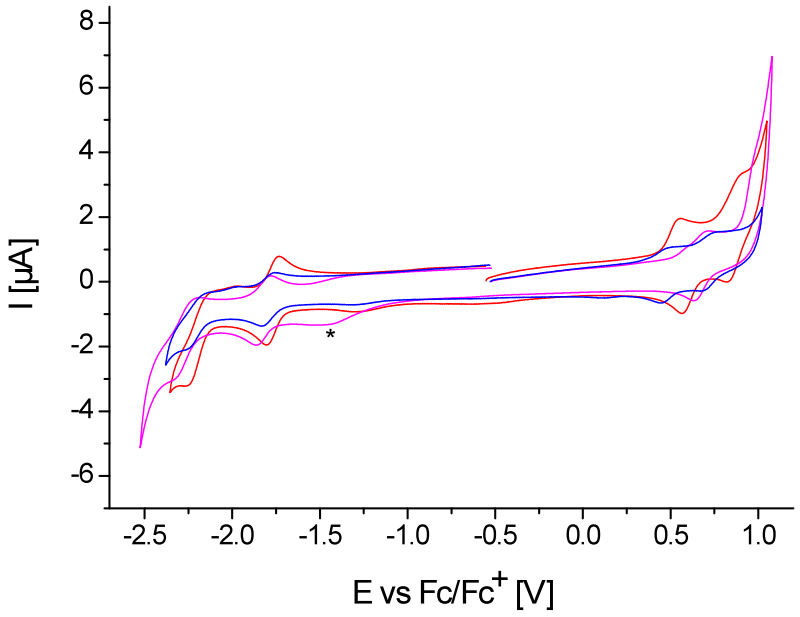

Figure S7. Cyclic voltammogram of **Cu-1** (red), **Pd-1** (magenta) and **Zn-1** (blue) in DCM containing 0.1 M TBAP (* impurity from the solvent)

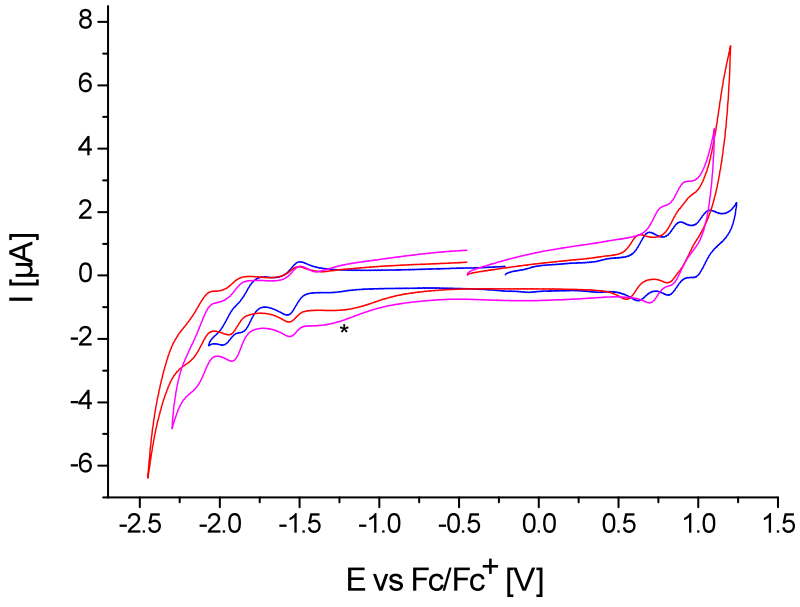

Figure S8. Cyclic voltammogram of **Cu-1-Ru** (red), **Pd-1-Ru** (magenta) and **H_2-1-Ru** (blue) in DCM containing 0.1 M TBAP (* impurity from the solvent)

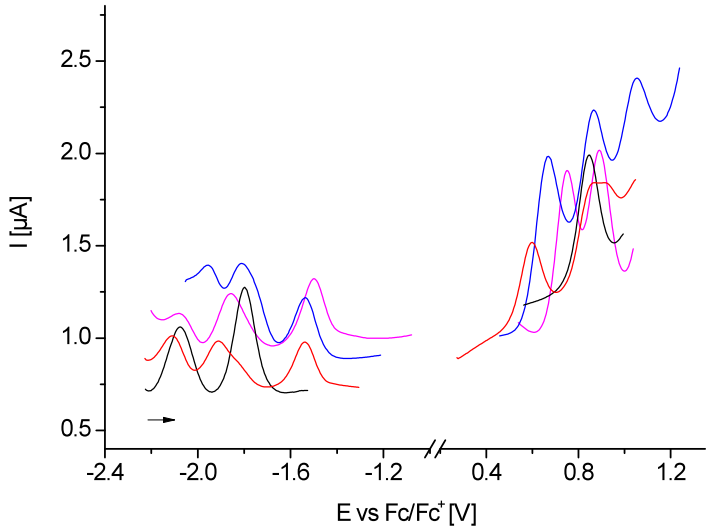

Figure S9. Square-wave voltammogram of $[Ru(tbbpy)_2(phen)](PF_6)_2$ (black), **Cu-1-Ru** (red), **Pd-1-Ru** (magenta) and **H_2-1-Ru** (blue) in DCM containing 0.1 M TBAP

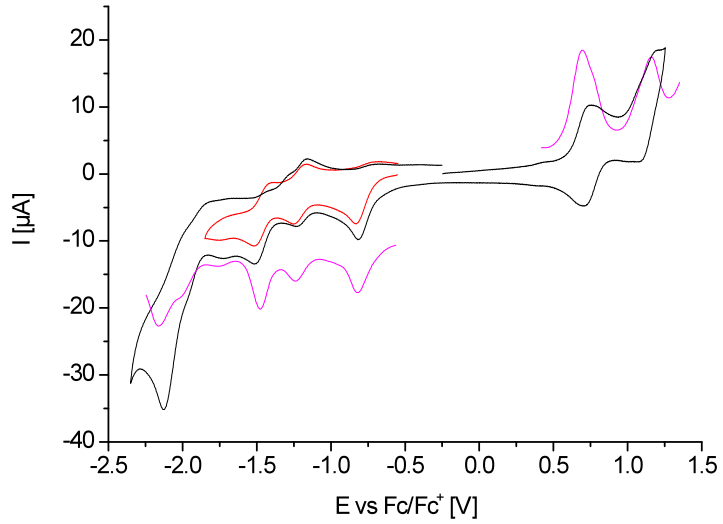

Figure S10. Cyclic voltammogram (black, red) and square-wave voltammogram (magenta) of **FeCl-1** in DCM containing 0.1 M TBAP

The CV of **FeCl-1** shows four reduction and two oxidation events in DCM. FeClTPP (Kadish, K. M.; Morrison, M. M.; Constant, L. A.; Dickens, L.; Davis, D. G. *J. Am. Chem. Soc.* **1976**, *98*, 8387-8390) exhibits two iron-based reductions in DCM followed by a porphyrin-based reduction. In DMF a similar behavior can be found (Lexa, D.; Momenteau, M; Rentien, P.; Rytz, G.; Savéant, J.-M.; Xu, F. *J. Am. Chem. Soc.* **1984**, *106*, 4755-4765). For **FeCl-1**, we assume that the first (irreversible) and second (quasi-reversible) reduction events are iron-based and the third (quasi-reversible) reduction is ligand-centered. CVs were run at different scan rates and with different reverse potentials to elucidate the reversible character of the redox events. The fourth (irreversible) reduction may correspond to the Fe^{I}/Fe^{0} couple but can also be ligand-based or both. At this point, we cannot clearly distinguish between these options.

Furthermore, FeClTPP exhibits two oxidation potentials, that were assigned to, first, an iron-based and, second, a ligand oxidation. For **FeCl-1**, the first oxidation event is also assigned to the Fe^{III}/Fe^{IV}-couple, which very likely overlays with the first macrocycle-centered oxidation. (The integration of this event in comparison to the second oxidation event is twice as high in the SQV (Figure S10) and a shoulder becomes visible, that means that two one-electron oxidation processes occur at a similar potential). The second oxidation event is probably ligand-based and involves the second macrocycle-centered oxidation.

Co-1 shows three reduction and two oxidation events (see table S2). The first reduction process is cobalt-based and irreversible, as described for CoTPP (Truxillo, L. A.; Davis, D. G. *Anal. Chem.* **1975**, *47*, 2260-2267) and the other two are very likely ligand-based. Further, for CoTPP, the first oxidation is metal-based followed by a porphyrin-based oxidation. Thus, for **Co-1**, we suggest that the first oxidation is also cobalt-centered and the second oxidation is then based on the ligand. No second ligand-based oxidation is found in the solvent window.

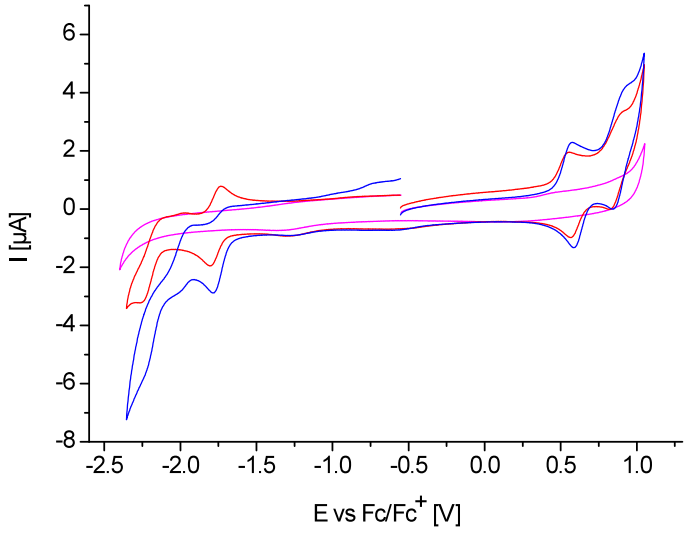

Figure S11. Cyclic voltammogram of **Cu-1** under argon atmosphere (red) and under CO_2 atmosphere (blue), and of the background without sample under CO_2 atmosphere (magenta) in DCM containing 0.1 M TBAP

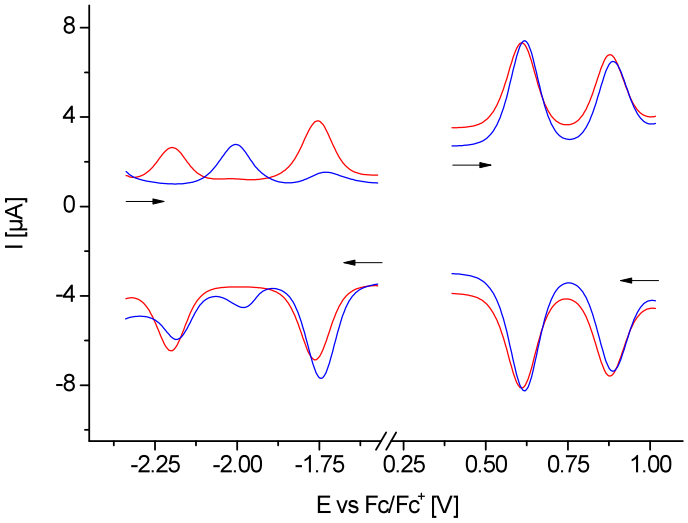

Figure S12: Square-wave voltammogram of **Cu-1** under argon atmosphere (red) and under CO_2 atmosphere (blue) in DCM containing 0.1 M TBAP

The cyclic voltammograms of **Cu-1** under argon and CO_2 atmosphere are shown in figure S11 and the corresponding square-wave voltammograms in figure S12. Obviously, the oxidation potentials do not shift while the reduction potentials are affected. There are two reversible reduction events under argon. Scanning cathodically under CO_2 atmosphere reveals a small shift of the first reduction event and the appearance of a small cathodic peak at -1.98 V that might indicate a CO_2 adduct that is formed. Afterwards the second reduction of **Cu-1** occurs and is irreversible, because the corresponding oxidation wave is missing. Instead a new anodic potential arises at more positive potential (-2.00 V) indicating an interaction of the double reduced species and CO_2 (and potentially some catalytic behavior). The first reduction of **Cu-1** scanned alone in a CV experiment is also reversible under CO_2 atmosphere. Thus, at least the double reduced species is required for an interaction between **Cu-1** and CO_2. It might be that in the double reduced state the copper center gets partially reduced to allow CO_2 coordination and reduction; however, this could not be experimentally proven yet.

Note, that CV experiments could not be executed in DMF due to low solubility of the compounds in this solvent and hence weak signals.

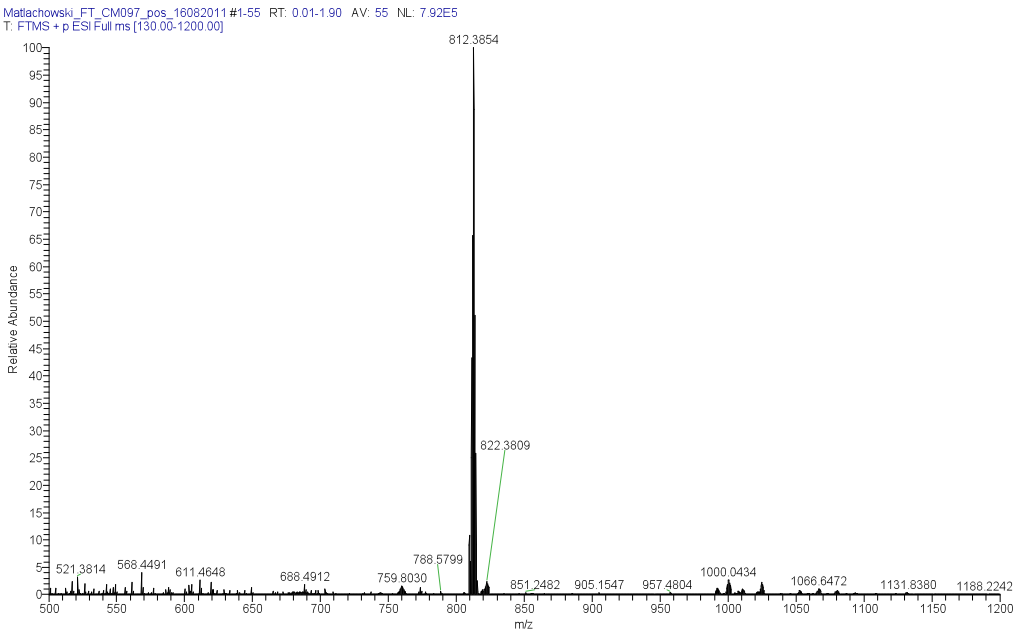

Figure S13. High-resolution ESI-MS of **H_2-1-Ru**

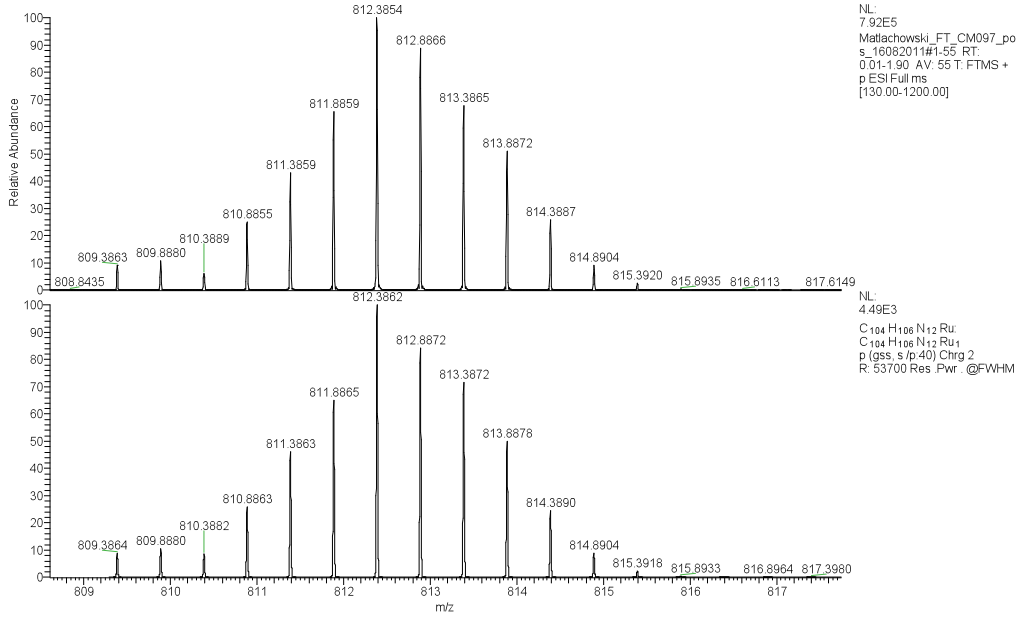

Figure S14. Measured (top) and calculated (bottom) isotopic pattern for the peak at m/z=812 in the high-resolution ESI-MS of **H_2-1-Ru**

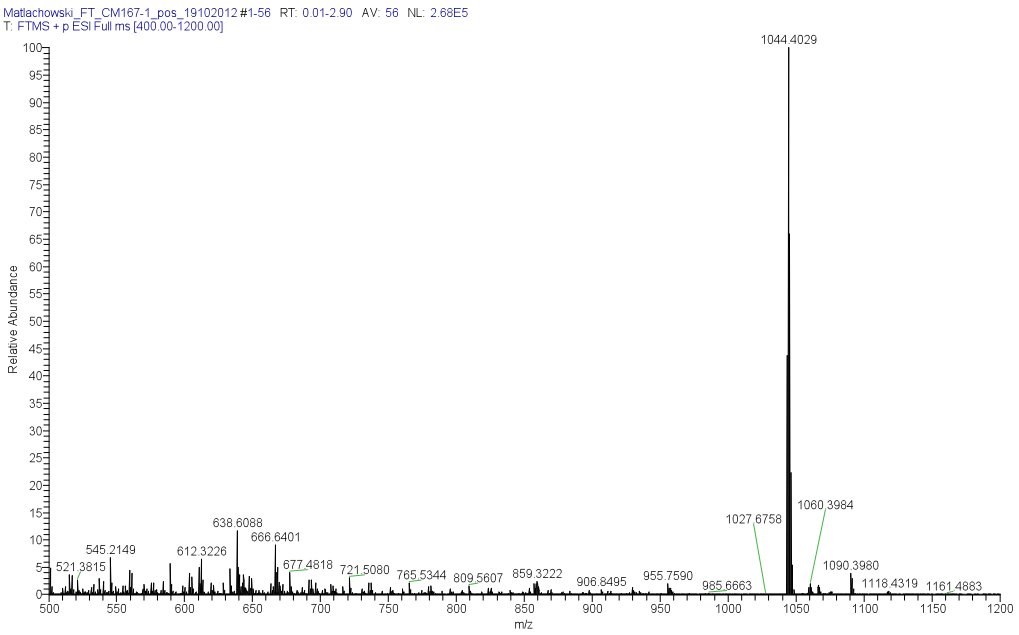

Figure S15. High-resolution ESI-MS of **Co-1**

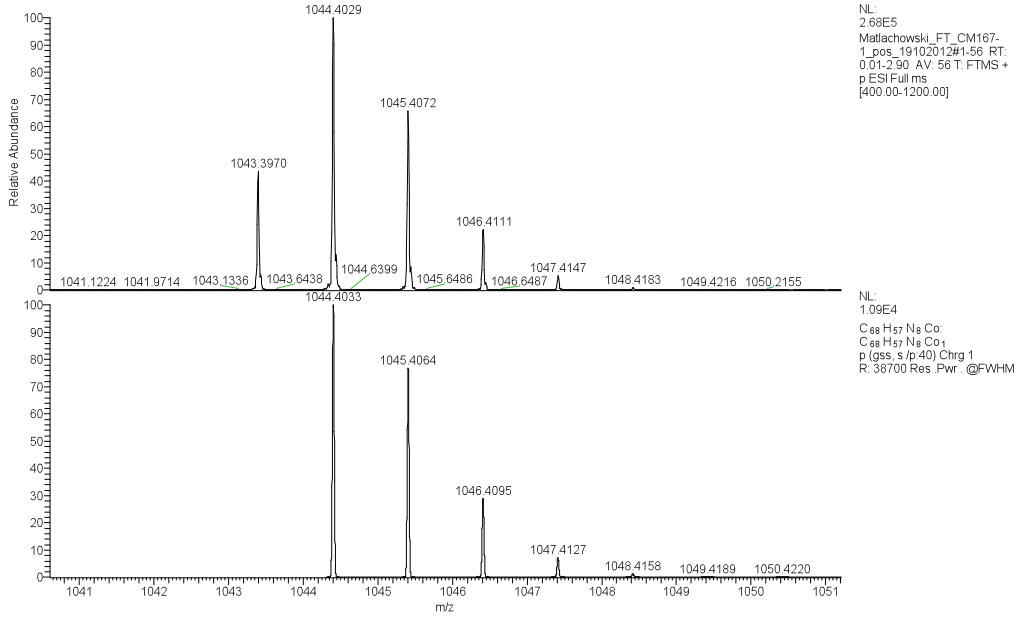

Figure S16. Measured (top) and calculated (bottom) isotopic pattern for the peak at m/z=1044 in the high-resolution ESI-MS of **Co-1**

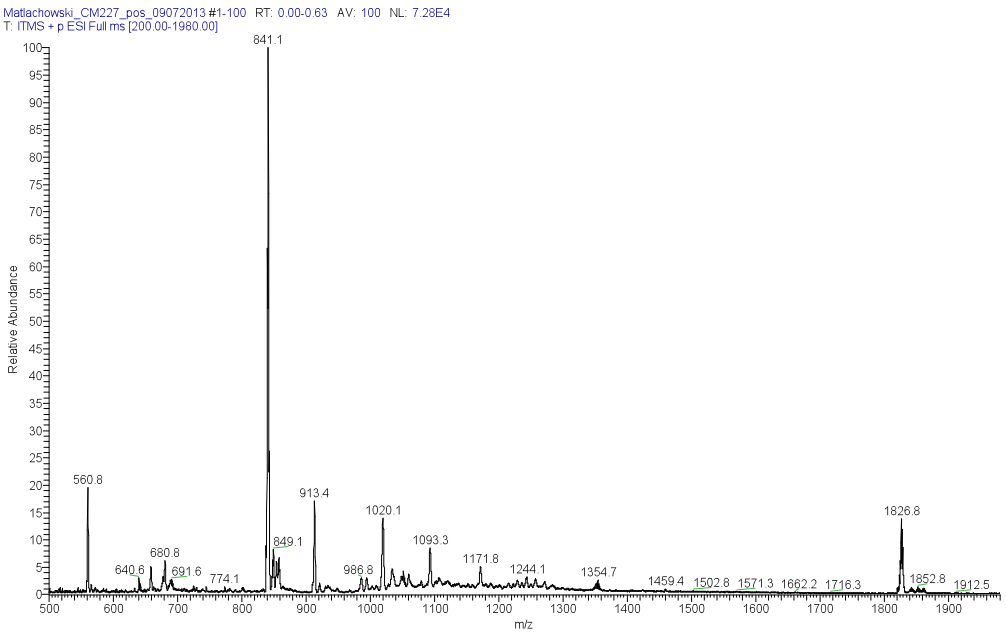

Figure S17. ESI-MS of **Co-1-Ru**

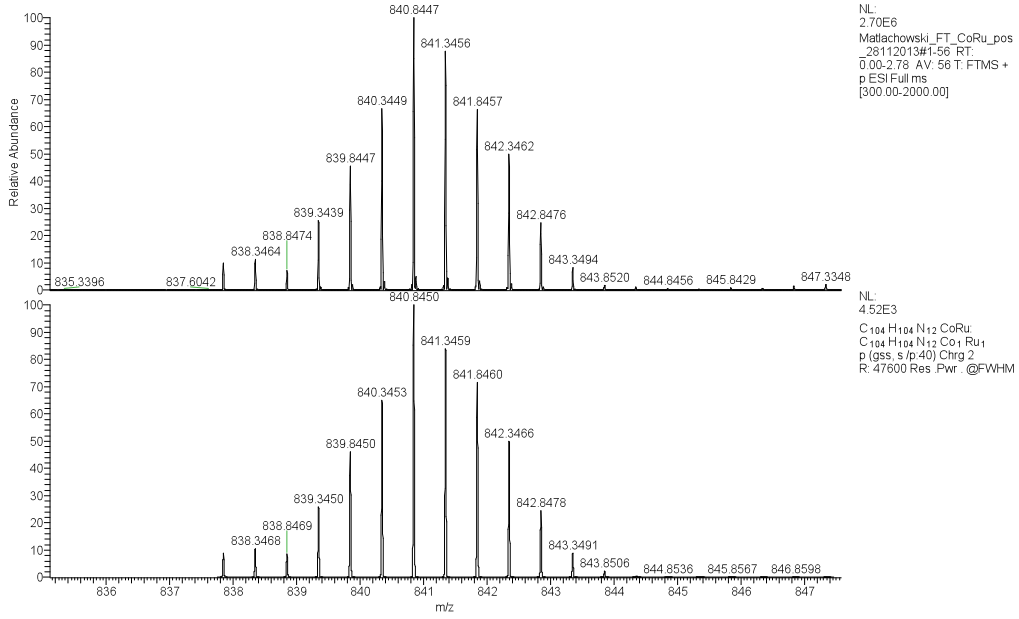

Figure S18. Measured (top) and calculated (bottom) isotopic pattern for the peak at m/z=841 in the high-resolution ESI-MS of **Co-1-Ru**

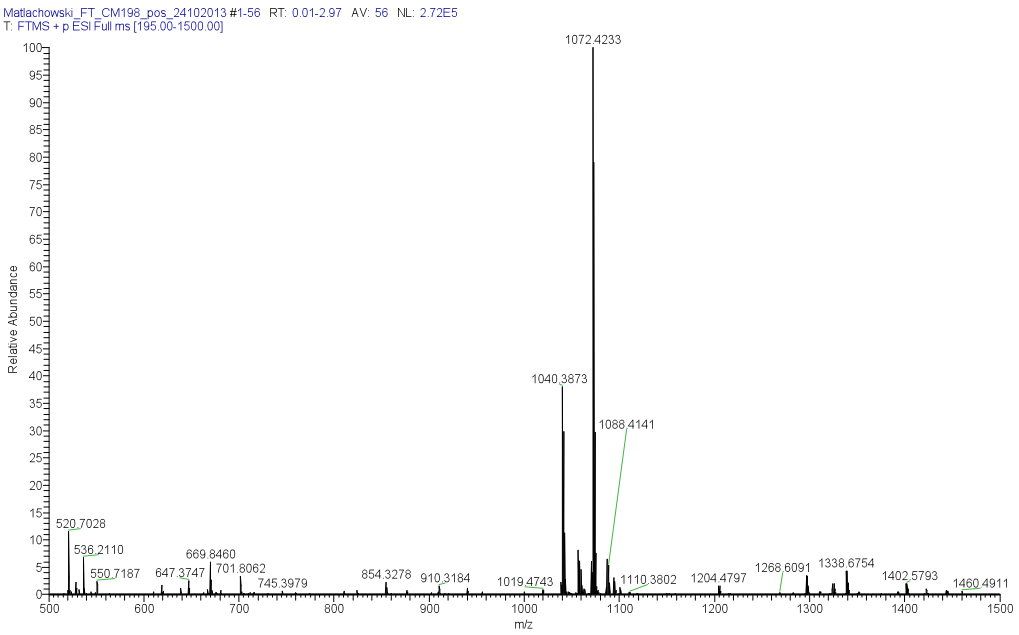

Figure S19. High-resolution ESI-MS of **FeCl-1**

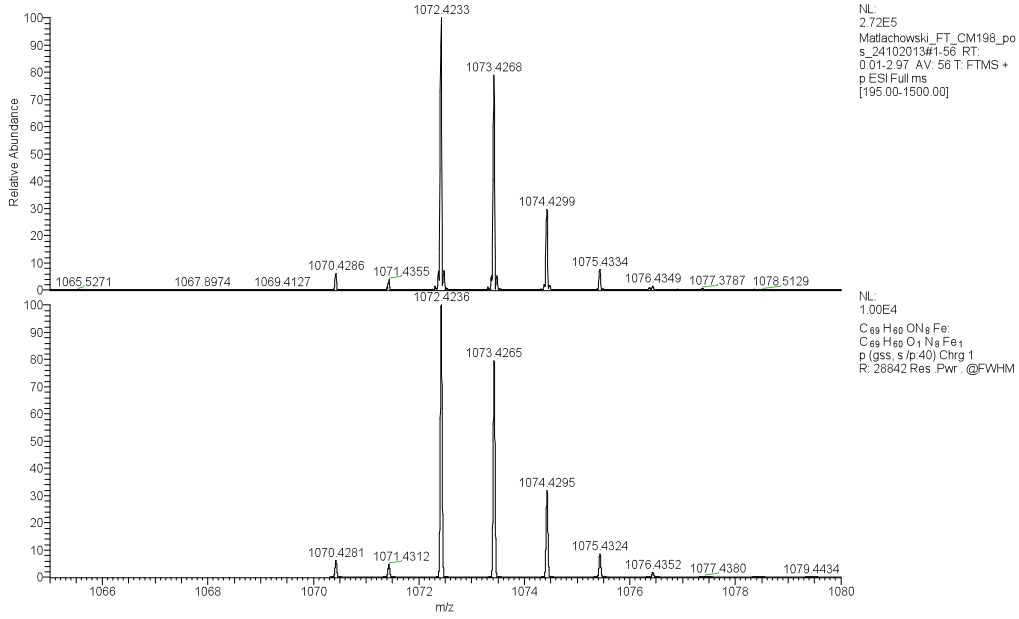

Figure S20. Measured (top) and calculated (bottom) isotopic pattern for the peak at m/z=1072 in the high-resolution ESI-MS of **FeCl-1**

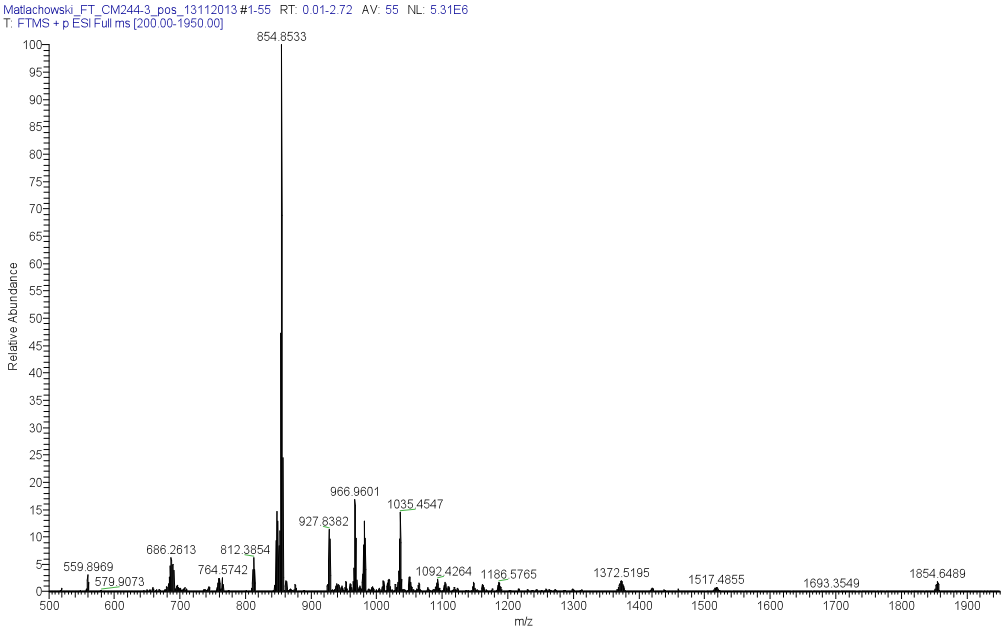

Figure S21. High-resolution ESI-MS of **FeCl-1-Ru**

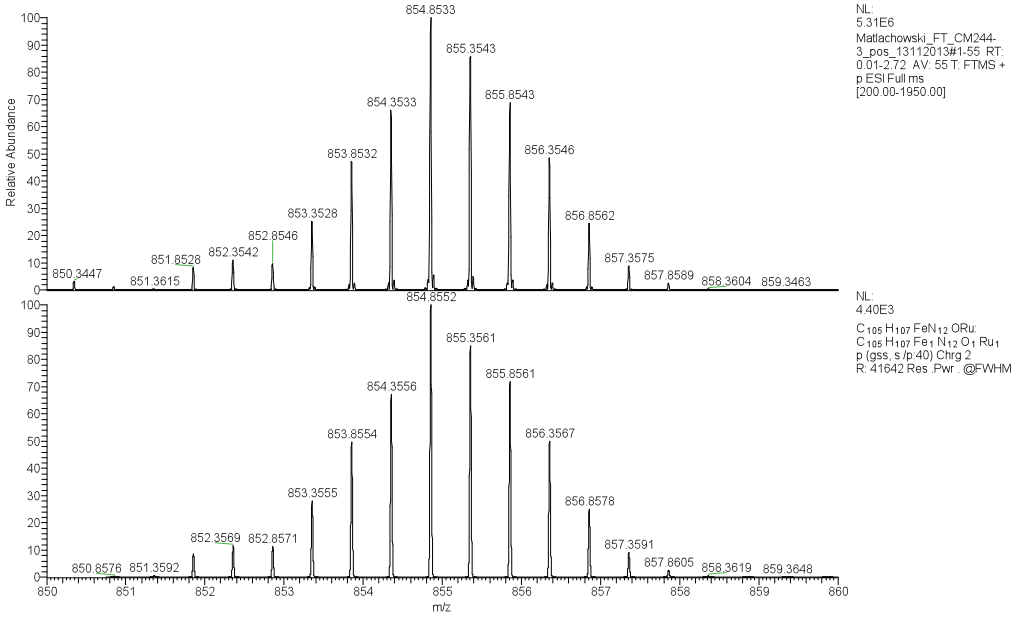

Figure S22. Measured (top) and calculated (bottom) isotopic pattern for the peak at m/z=854 in the high-resolution ESI-MS of **FeCl-1-Ru**

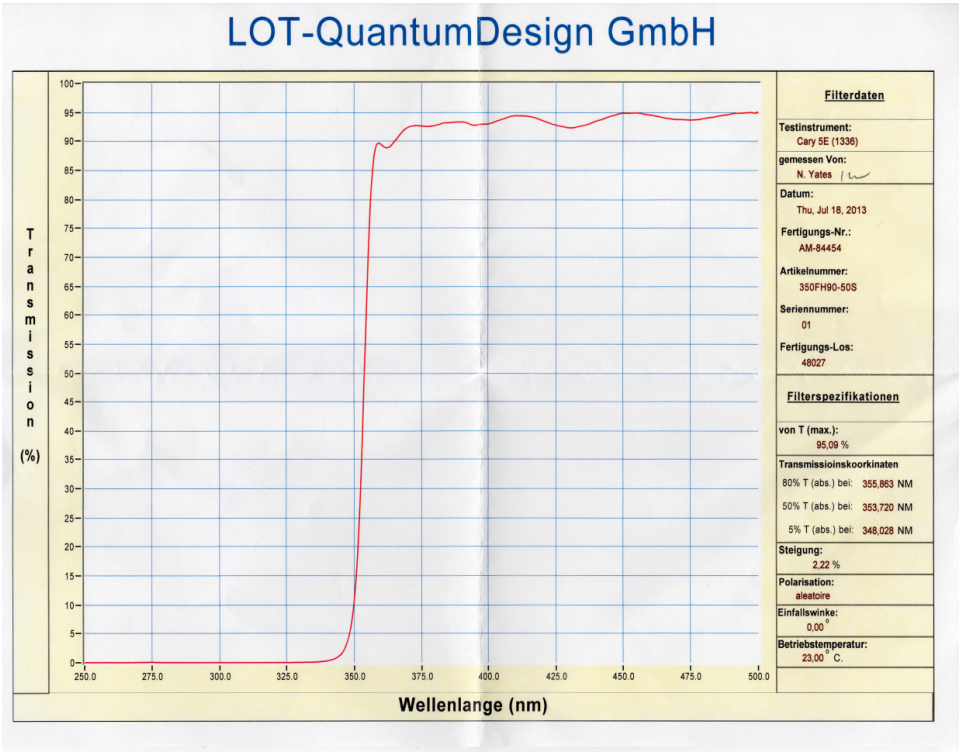

Figure S23: Transmission spectrum of the 350 nm long-wave pass cut-off filter. All other filters used show the same edge (transmission) profile.